CHINESE JOURNAL OF MECHANICAL ENGINEERING
Vol. 27, No. 5, 2014

DOI: 10.3901/CJME.2014.0618.113, available online at www.springerlink.com; www.cjmenet.com; www.cjmenet.com.cn

# Running Accuracy Analysis of a 3-RRR Parallel Kinematic Machine Considering the Deformations of the Links

WANG Liping, JIANG Yao*, and LI Tiemin

*Department of Mechanical Engineering, Tsinghua University, Beijing 100084, China*

Received October 31, 2013; revised June 3, 2014; accepted June 18, 2014

**Abstract:** Parallel kinematic machines have drawn considerable attention and have been widely used in some special fields. However, high precision is still one of the challenges when they are used for advanced machine tools. One of the main reasons is that the kinematic chains of parallel kinematic machines are composed of elongated links that can easily suffer deformations, especially at high speeds and under heavy loads. A 3-RRR parallel kinematic machine is taken as a study object for investigating its accuracy with the consideration of the deformations of its links during the motion process. Based on the dynamic model constructed by the Newton-Euler method, all the inertia loads and constraint forces of the links are computed and their deformations are derived. Then the kinematic errors of the machine are derived with the consideration of the deformations of the links. Through further derivation, the accuracy of the machine is given in a simple explicit expression, which will be helpful to increase the calculating speed. The accuracy of this machine when following a selected circle path is simulated. The influences of magnitude of the maximum acceleration and external loads on the running accuracy of the machine are investigated. The results show that the external loads will deteriorate the accuracy of the machine tremendously when their direction coincides with the direction of the worst stiffness of the machine. The proposed method provides a solution for predicting the running accuracy of the parallel kinematic machines and can also be used in their design optimization as well as selection of suitable running parameters.

**Keywords:** parallel kinematic machine, dynamic model, accuracy, deformations

## 1 Introduction

Compared with serial machines, parallel kinematic machines(PKMs) have advantages in terms of high stiffness, excellent dynamic performance, large payload, and ease of control[1–2]. Therefore, they are increasingly being used in the industry, for example as machine tools, assembly robots, flight simulators, or radio telescopes[3–5]. The earliest PKMs were based on hexapods[6] which, at least in theory, are more precise than serial machines, as they do not suffer from error accumulation[7]. However, this is not the case in practice, where none of them are more accurate than conventional serial machine tools[8]. The main reason is that it is difficult to ensure the manufacturing accuracy of the spatial joints.

To overcome this problem, planar PKMs have been introduced and have created considerable interest[9]. Their components are all jointed together by revolute or prismatic joints, which are much easier to manufacture with high accuracy. However, only few planar PKMs are used in high accuracy applications with success[10]. Though a number of inevitable errors exist in the process of manufacturing and assembling, they can be calculated and compensated for through kinematic calibration[11–12]. With further research, it has been found that the elongated links of PKMs can easily suffer from deformations during the motion process[13], especially at high speeds or under heavy loads. The deformations of the links are changing dynamically and are impossible to eliminate in advance. In order to reduce their deformations, the links can be designed to be more rigid, but this would increase their inertia and decrease the dynamic performance of the machine[14].

In order to improve the accuracy of the PKM during the motion process, it is necessary to study the kinematic errors of the machine caused by the deformations of its links. Then it can be possible to seek the solutions for improving the running accuracy of the machine, such as design optimization, suitable running parameters selection and so on. First of all, the dynamic model of the machine with the flexible components should be studied. Recently, the dynamics of flexible serial machines has been studied by many researchers[15], and numerous approaches were developed to predict their dynamic characteristics. By contrast, PKMs have relatively complicated kinematic and dynamic performance. A few investigations were concerned with the dynamics of flexible PKMs. PIRAS, et al[16],

* Corresponding author. E-mail: jiangyao11@mails.tsinghua.edu.cn
Supported by National Natural Science Foundation of China(Grant No. 51272560), National Basic Research Program of China(973 Program, Grant No. 2011CB302404), and National Science Foundation for Distinguished Young Scholars of China(Grant No. 51225503)

studied the dynamics of a planar fully parallel robot with flexible links by the finite element method. The results showed that the configuration of the mechanism had a significant influence on the nature of the resulting elastic vibrations. ZHANG, et al[17], developed the structural dynamic equations of motion for a 3-PRRR parallel manipulator with three flexible intermediate links based on the assumed mode method. The modal characteristics of the flexible manipulator system were given. WANG, et al[18], utilized the Lagrange finite element formulation to derive the dynamic model for a flexible planar linkage of a planar parallel manipulator. Based on the dynamic model, PZT actuators were applied to effectively damp vibration of the flexible linkages. ZHOU et al[19], provided a vibration analysis model and the modeling method for a fully flexible 3PRS manipulator. In their work, the foci are mainly on the vibration analysis of the flexible parallel kinematic machines. The accuracy of the machines and the corresponding influence factors, such as running parameters and external loads are not considered. There are some other articles in the literature investigating the accuracy analysis of the PKMs. Several performance indices were developed to roughly evaluate their accuracy, including a dexterity index[20], condition numbers and a global conditioning index[21]. The best accuracy measures included the local maximum position and orientation errors, given actuator inaccuracies, and mean value and variance of the errors over a specific workspace[22–24]. However, those indices are not suitable for analyzing the PKMs with both translational and rotational degrees of freedom[25]. Moreover, the dynamic characteristic of the machine and the flexibility of the links are not taken into account in these investigations.

In this paper, the 3-RRR PKM[26–28], a typical planar machine performing two translational and one rotational motions, is mainly discussed as the study object. Based on the dynamic model, a novel method is presented to analyze its running accuracy with the consideration of the deformations of its links. The remainder of this paper is organized as follows. In section 2, the inverse kinematics of this machine is analyzed. Then its dynamic model is constructed by the Newton-Euler method in section 3. In section 4, the deformations of all links under constraint forces and inertia forces are calculated. In section 5, the relationship between the accuracy of the machine and the deformations of the links is established. In section 6, numerical examples are presented. Finally, conclusions are given.

## 2 Description and Inverse Kinematic Model

As shown in Fig. 1, the 3-RRR PKM is composed of a base, a moving platform and three identical kinematic chains. Each kinematic chain consists of two links jointed together by a revolute joint, and with one end connected to the base at point $A_i$ and the other end connected to the moving platform at point $C_i$ by revolute joints. The machine possesses three degrees of freedom and is actuated by three motors located at points $A_1$, $A_2$ and $A_3$.

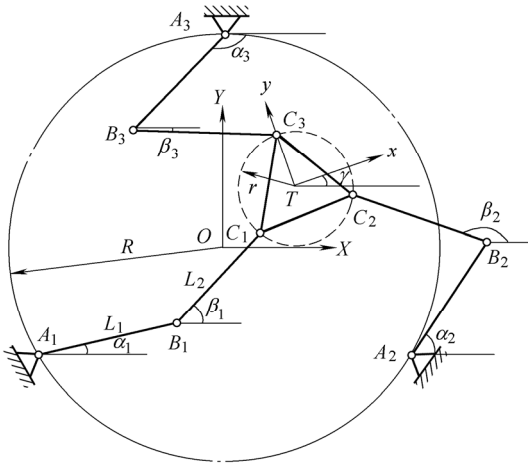


Fig. 1. Kinematic model of a 3-RRR PKM

As illustrated in Fig. 2, a base coordinate frame $OXYZ$ is fixed to the base and a moving coordinate frame $Txyz$ is attached to the moving platform. Another two moving frames $A_ix_iy_iz_i$ and $B_ix_iy_iz_i$ are mounted on links $A_iB_i$ and $B_iC_i$ at points $A_i$ and $B_i$, respectively.

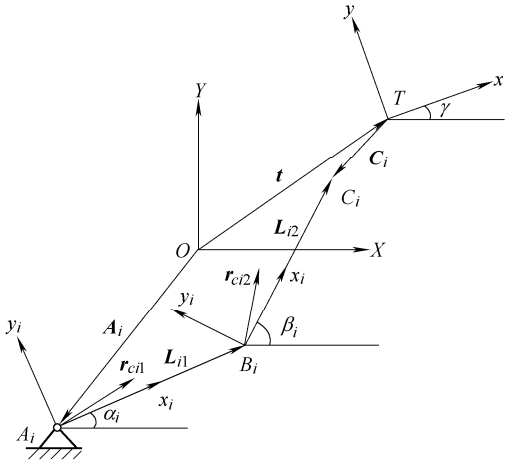


Fig. 2. Vector loop of a kinematic chain

The rotation matrices of coordinate frames $\{T\}$, $\{A_i\}$ and $\{B_i\}$ with respect to $\{O\}$ can be described respectively as

$$ {}^{O}\boldsymbol{R}_{T} = \begin{pmatrix} \cos\gamma & -\sin\gamma & 0 \\ \sin\gamma & \cos\gamma & 0 \\ 0 & 0 & 1 \end{pmatrix}, \tag{1} $$

$$ {}^{O}\boldsymbol{R}_{Ai} = \begin{pmatrix} \cos\alpha_i & -\sin\alpha_i & 0 \\ \sin\alpha_i & \cos\alpha_i & 0 \\ 0 & 0 & 1 \end{pmatrix}, \tag{2} $$

$$ {}^{O}\boldsymbol{R}_{Bi} = \begin{pmatrix} \cos\beta_i & -\sin\beta_i & 0 \\ \sin\beta_i & \cos\beta_i & 0 \\ 0 & 0 & 1 \end{pmatrix}, \tag{3} $$

where $\alpha_i$, $\beta_i$ and $\gamma$ are the rotation angles of link $A_iB_i$, link $B_iC_i$ and the moving platform, respectively.

According to Fig. 2, the closed-loop constraint equation associated with the $i$th kinematic chain can be written as

$$\boldsymbol{t} + {}^{O}\boldsymbol{R}_{T}\,{}^{T}\boldsymbol{C}_i = \boldsymbol{A}_i + L_1\boldsymbol{l}_{i1} + L_2\boldsymbol{l}_{i2}, \tag{4}$$

where $\boldsymbol{t}=(x\ y\ 0)^{\mathrm{T}}$, ${}^{T}\boldsymbol{C}_i=(x_{Ci}\ y_{Ci}\ 0)^{\mathrm{T}}$, and $\boldsymbol{A}_i=(x_{Ai}\ y_{Ai}\ 0)^{\mathrm{T}}$ are the position vectors of points $T$, $C_i$ and $A_i$ in coordinate frames $\{O\}$, $\{T\}$ and $\{O\}$, respectively. $L_1$ and $L_2$ are the length of links $A_iB_i$ and $B_iC_i$, and $\boldsymbol{l}_{i1}$ and $\boldsymbol{l}_{i2}$ are their unit vectors.

For a given $\boldsymbol{t}$, taking the norm on both sides of Eq. (4) yields

$$L_2 = \left\| \boldsymbol{t} + {}^{O}\boldsymbol{R}_{T}\,{}^{T}\boldsymbol{C}_i - \boldsymbol{A}_i - L_1\boldsymbol{l}_{i1} \right\|. \tag{5}$$

The only unknown in Eq. (5) is $\alpha_i$, which can be solved uniquely[28] according to the assembly model in Fig. 1 and unit vector $\boldsymbol{l}_{i1}$ can be determined consequently.

From Eq. (4), unit vector $\boldsymbol{l}_{i2}$ can be derived as

$$\boldsymbol{l}_{i2} = \frac{1}{L_2}\left(\boldsymbol{t} + {}^{O}\boldsymbol{R}_{T}\,{}^{T}\boldsymbol{C}_i - \boldsymbol{A}_i - L_1\boldsymbol{l}_{i1}\right). \tag{6}$$

The position vectors of centroids $c_{i1}$ and $c_{i2}$ of links $A_iB_i$ and $B_iC_i$ in coordinate frame $\{O\}$ can be expressed as

$$\boldsymbol{r}_{ci1} = \boldsymbol{A}_i + {}^{O}\boldsymbol{R}_{Ai}\,{}^{Ai}\boldsymbol{r}_{ci1}, \tag{7}$$

$$\boldsymbol{r}_{ci2} = \boldsymbol{A}_i + L_1\boldsymbol{l}_{i1} + {}^{O}\boldsymbol{R}_{Bi}\,{}^{Ai}\boldsymbol{r}_{ci2}, \tag{8}$$

where ${}^{Ai}\boldsymbol{r}_{ci1} = \frac{L_1}{2}(1\ 0\ 0)^{\mathrm{T}}$, ${}^{Bi}\boldsymbol{r}_{ci2} = \frac{L_2}{2}(1\ 0\ 0)^{\mathrm{T}}$.

Taking the time derivative of Eq. (4) leads to

$$\boldsymbol{v}_T + \boldsymbol{\omega}\times\left({}^{O}\boldsymbol{R}_{T}\,{}^{T}\boldsymbol{C}_i\right) = \boldsymbol{\omega}_{i1}\times\left(L_1\boldsymbol{l}_{i1}\right) + \boldsymbol{\omega}_{i2}\times\left(L_2\boldsymbol{l}_{i2}\right), \tag{9}$$

where $\boldsymbol{v}_T$ is the velocity of point $T$, and $\boldsymbol{\omega}$, $\boldsymbol{\omega}_{i1}$ and $\boldsymbol{\omega}_{i2}$ are the angular velocities of the moving platform, links $A_iB_i$ and $B_iC_i$, respectively.

Taking the dot product with $\boldsymbol{l}_{i2}$ and $\boldsymbol{l}_{i1}$ respectively on both sides of Eq. (9) yields

$$\omega_{i1} = \frac{\boldsymbol{l}_{i2}\cdot\left(\boldsymbol{v}_T + \boldsymbol{\omega}\times\left({}^{O}\boldsymbol{R}_{T}\,{}^{T}\boldsymbol{C}_i\right)\right)}{L_1\boldsymbol{e}_3\cdot\left(\boldsymbol{l}_{i1}\times\boldsymbol{l}_{i2}\right)}, \tag{10}$$

$$\omega_{i2} = \frac{\boldsymbol{l}_{i1}\cdot\left(\boldsymbol{v}_T + \boldsymbol{\omega}\times\left({}^{O}\boldsymbol{R}_{T}\,{}^{T}\boldsymbol{C}_i\right)\right)}{L_2\boldsymbol{e}_3\cdot\left(\boldsymbol{l}_{i2}\times\boldsymbol{l}_{i1}\right)}. \tag{11}$$

Taking the time derivative of Eqs. (7) and (8), the velocities of points $c_{i1}$ and $c_{i2}$ can be obtained as

$$\boldsymbol{v}_{ci1} = \boldsymbol{\omega}_{i1}\times\left({}^{O}\boldsymbol{R}_{Ai}\,{}^{Ai}\boldsymbol{r}_{ci1}\right), \tag{12}$$

$$\boldsymbol{v}_{ci2} = \boldsymbol{\omega}_{i1}\times\left(L_1\boldsymbol{l}_{i1}\right) + \boldsymbol{\omega}_{i2}\times\left({}^{O}\boldsymbol{R}_{Bi}\,{}^{Bi}\boldsymbol{r}_{ci2}\right). \tag{13}$$

Differentiating Eq. (9) with respect to time yields

$$\boldsymbol{a}_T + \boldsymbol{\varepsilon}\times\left({}^{O}\boldsymbol{R}_{T}\,{}^{T}\boldsymbol{C}_i\right) - \omega^2\left({}^{O}\boldsymbol{R}_{T}\,{}^{T}\boldsymbol{C}_i\right) =$$
$$\boldsymbol{\varepsilon}_{i1}\times\left(L_1\boldsymbol{l}_{i1}\right) - \omega_{i1}^2 L_1\boldsymbol{l}_{i1} + \boldsymbol{\varepsilon}_{i2}\times\left(L_2\boldsymbol{l}_{i2}\right) - \omega_{i2}^2 L_2\boldsymbol{l}_{i2}, \tag{14}$$

where $\boldsymbol{a}_T$ is the acceleration of point $T$, and $\boldsymbol{\varepsilon}$, $\boldsymbol{\varepsilon}_{i1}$ and $\boldsymbol{\varepsilon}_{i2}$ are the angular accelerations of the moving platform, links $A_iB_i$ and $B_iC_i$, respectively.

Through the same method as above, the magnitude of the angular accelerations of links $A_iB_i$ and $B_iC_i$, and the accelerations of points $c_{i1}$ and $c_{i2}$ can be obtained respectively as

$$\varepsilon_{i1} = \frac{\boldsymbol{l}_{i2}\cdot\left(\boldsymbol{a}_T + \boldsymbol{\varepsilon}\times\boldsymbol{C}_i - \omega^2\boldsymbol{C}_i + \omega_{i1}^2 L_1\boldsymbol{l}_{i1} + \omega_{i2}^2 L_2\boldsymbol{l}_{i2}\right)}{L_1\left(\boldsymbol{l}_{i1}\times\boldsymbol{l}_{i2}\right)}, \tag{15}$$

$$\varepsilon_{i2} = \frac{\boldsymbol{l}_{i1}\cdot\left(\boldsymbol{a}_T + \boldsymbol{\varepsilon}\times\boldsymbol{C}_i - \omega^2\boldsymbol{C}_i + \omega_{i1}^2 L_1\boldsymbol{l}_{i1} + \omega_{i2}^2 L_2\boldsymbol{l}_{i2}\right)}{L_2\left(\boldsymbol{l}_{i2}\times\boldsymbol{l}_{i1}\right)}, \tag{16}$$

$$\boldsymbol{a}_{ci1} = \boldsymbol{\varepsilon}_{i1}\times\left({}^{O}\boldsymbol{R}_{Ai}\,{}^{Ai}\boldsymbol{r}_{ci1}\right) - \omega_{i1}^2\,{}^{O}\boldsymbol{R}_{Ai}\,{}^{Ai}\boldsymbol{r}_{ci1}, \tag{17}$$

$$\boldsymbol{a}_{ci2} = \boldsymbol{\varepsilon}_{i1}\times\left(L_1\boldsymbol{l}_{i1}\right) - \omega_{i1}^2 L_1\boldsymbol{l}_{i1} +$$
$$\boldsymbol{\varepsilon}_{i2}\times\left({}^{O}\boldsymbol{R}_{Bi}\,{}^{Bi}\boldsymbol{r}_{ci2}\right) - \omega_{i1}^2\,{}^{O}\boldsymbol{R}_{Bi}\,{}^{Bi}\boldsymbol{r}_{ci2}. \tag{18}$$

## 3 Inverse Dynamic Model

In order to analyze the kinematic errors of the moving platform caused by the deformations of the links, all the applied forces should be computed. Therefore, the dynamic model of the machine is constructed by utilizing the Newton-Euler method. The force analysis diagrams of link $B_iC_i$, link $A_iB_i$ and the moving platform are shown in Figs. 3, 4 and 5, respectively.

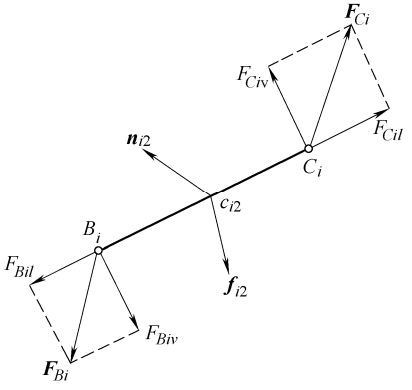


Fig. 3. Force analysis diagram of link $B_iC_i$

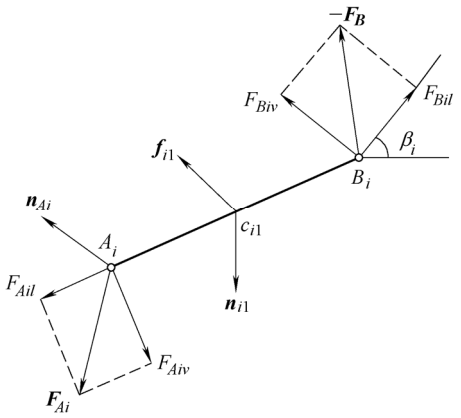


Fig. 4. Force analysis diagram of link $A_iB_i$

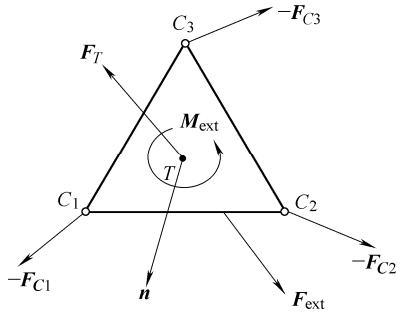


Fig. 5. Force analysis diagram of the moving platform

According to Fig. 3, the force balance equation of link $B_iC_i$ can be expressed as

$$\boldsymbol{F}_{Bi}+\boldsymbol{F}_{Ci}+\boldsymbol{f}_{i2}=\boldsymbol{0}, \tag{19}$$

where $\boldsymbol{f}_{i2}=-m_2\boldsymbol{a}_{ci2}$ is the inertial force of link $B_iC_i$, $m_2$ is its mass, and $\boldsymbol{F}_{Bi}=(F_{Biv}\ F_{Bil}\ 0)^{\mathrm{T}}$ and $\boldsymbol{F}_{Ci}=(F_{Civ}\ F_{Cil}\ 0)^{\mathrm{T}}$ represent the constraint forces at points $B_i$ and $C_i$.

Taking moment about points $B_i$ and $C_i$, the moment balance equations of link $B_iC_i$ can be obtained as

$$\left({}^{O}\boldsymbol{R}_{Bi}\,{}^{Bi}\boldsymbol{r}_{ci2}\right)\times\boldsymbol{f}_{i2}+L_2\boldsymbol{l}_{i2}\times\boldsymbol{F}_{Ci}+\boldsymbol{n}_{i2}=\boldsymbol{0}, \tag{20}$$

$$\left({}^{O}\boldsymbol{R}_{Bi}\,{}^{Bi}\boldsymbol{r}_{ci2}-L_2\boldsymbol{l}_{i2}\right)\times\boldsymbol{f}_{i2}-L_2\boldsymbol{l}_{i2}\times\boldsymbol{F}_{Bi}+\boldsymbol{n}_{i2}=\boldsymbol{0}, \tag{21}$$

where $\boldsymbol{n}_{i2}=-\boldsymbol{J}_2\boldsymbol{\varepsilon}_{i2}$ is the inertial moment of link $B_iC_i$, and $\boldsymbol{J}_2$ is its moment of inertia.

From Eqs. (20) and (21), $F_{Civ}$ and $F_{Biv}$ can be obtained as

$$F_{Civ}=-\boldsymbol{e}_3\bullet\left(\left({}^{O}\boldsymbol{R}_{Bi}\,{}^{Bi}\boldsymbol{r}_{ci2}\right)\times\boldsymbol{f}_{i2}+\boldsymbol{n}_{i2}\right)\Big/L_2, \tag{22}$$

$$F_{Biv}=-\boldsymbol{e}_3\bullet\left(\left({}^{O}\boldsymbol{R}_{Bi}\,{}^{Bi}\boldsymbol{r}_{ci2}-L_2\boldsymbol{l}_{i2}\right)\times\boldsymbol{f}_{i2}+\boldsymbol{n}_{i2}\right)\Big/L_2. \tag{23}$$

According to Fig. 4, the force balance equation of link $A_iB_i$ can be described as

$$\boldsymbol{F}_{Ai}-\boldsymbol{F}_{Bi}+\boldsymbol{f}_{i1}=\boldsymbol{0}, \tag{24}$$

where $\boldsymbol{f}_{i1}=-m_1\boldsymbol{a}_{ci1}$ is the inertial force of link $A_iB_i$, $m_1$ is its mass, and $\boldsymbol{F}_{Ai}=(F_{Aiv}\ F_{Ail}\ 0)^{\mathrm{T}}$ represents the constraint force at point $A_i$.

Taking moment about point $A_i$ leads to

$$\left({}^{O}\boldsymbol{R}_{Ai}\,{}^{Ai}\boldsymbol{r}_{ci1}\right)\times\boldsymbol{f}_{i1}-L_1\boldsymbol{l}_{i1}\times\boldsymbol{F}_{Bi}+\boldsymbol{n}_{i1}+\boldsymbol{n}_{Ai}=\boldsymbol{0}, \tag{25}$$

where $\boldsymbol{n}_{i1}=-\boldsymbol{J}_1\boldsymbol{\varepsilon}_{i1}$ is the inertial moment of the link, $\boldsymbol{J}_1$ is its moment of inertia, and $\boldsymbol{n}_{Ai}$ is the driving torque.

Referring to Fig. 5, the force balance equation of the moving platform can be described as

$$\boldsymbol{F}_{\text{ext}}+\boldsymbol{F}_T-\sum_{i=1}^{3}\boldsymbol{F}_{Ci}=\boldsymbol{0}, \tag{26}$$

where $\boldsymbol{F}_T=-m\boldsymbol{a}_T$ is the inertial force of the moving platform, $m$ is its mass, and $\boldsymbol{F}_{\text{ext}}=(F_{\text{ext}x}\ F_{\text{ext}y}\ 0)^{\mathrm{T}}$ is the external force acting on the moving platform.

Taking moment about point $T$ leads to

$$\boldsymbol{M}_{\text{ext}}+\boldsymbol{R}\times\boldsymbol{F}_T-\sum_{i=1}^{3}\left({}^{O}\boldsymbol{R}_T\,{}^{T}\boldsymbol{C}_i\right)\times\boldsymbol{F}_{Ci}+\boldsymbol{n}=\boldsymbol{0}, \tag{27}$$

where $\boldsymbol{M}_{\text{ext}}$ is the external moment acting on the moving platform, $\boldsymbol{R}=(R_x\ R_y\ 0)^{\mathrm{T}}$ is the position vector of the mass center of the moving platform in coordinate frame $\{O\}$, $\boldsymbol{n}=-\boldsymbol{J}\boldsymbol{\varepsilon}$ is the inertial moment of the moving platform, and $\boldsymbol{J}$ is its moment of inertia.

Combining Eqs. (26) and (27) yields

$$\boldsymbol{P}\left(F_{C1l}\quad F_{C2l}\quad F_{C3l}\right)^{\mathrm{T}}=\boldsymbol{Q}, \tag{28}$$

where

$$\boldsymbol{P}=\begin{pmatrix}l_{12x} & l_{22x} & l_{32x}\\ l_{12y} & l_{22y} & l_{32y}\\ u_1 & u_2 & u_3\end{pmatrix},$$

$$\boldsymbol{Q}=\begin{pmatrix}F_{\text{ext}x}-ma_{Tx}+\sum_{i=1}^{3}l_{i2y}F_{Civ}\\ F_{\text{ext}y}-ma_{Ty}-\sum_{i=1}^{3}l_{i2x}F_{Civ}\\ M_{\text{ext}}+R_ yma_{Tx}-R_xma_{Ty}-\boldsymbol{e}_3\bullet\left(\boldsymbol{J}\boldsymbol{\varepsilon}\right)-\sum_{i=1}^{3}q_i\,F_{Civ}\end{pmatrix},$$

$$u_i=\boldsymbol{e}_3\bullet\left(\left({}^{O}\boldsymbol{R}_T\,{}^{T}\boldsymbol{C}_i\right)\times\boldsymbol{l}_{i2}\right),$$

$$q_i=\boldsymbol{e}_3\bullet\left(\left({}^{O}\boldsymbol{R}_T\,{}^{T}\boldsymbol{C}_i\right)\bullet\boldsymbol{l}_{i2}\right).$$

From Eq. (28), $F_{Cil}$ can be obtained as

$$\left(F_{C1l}\quad F_{C2l}\quad F_{C3l}\right)^{\mathrm{T}}=\boldsymbol{P}^{-1}\boldsymbol{Q}. \tag{29}$$

Then $\boldsymbol{F}_{Bi}$ can be obtained according to Eq. (19) as

$$\boldsymbol{F}_{Bi} = -\boldsymbol{F}_{Ci} - \boldsymbol{f}_{i2}. \tag{30}$$

The driving torque $\boldsymbol{n}_{Ai}$ can be obtained from Eq. (25) as

$$\boldsymbol{n}_{Ai} = -\left({}^{O}\boldsymbol{R}_{Ai}\,{}^{Ai}\boldsymbol{r}_{ci1}\right)\times \boldsymbol{f}_{i1} + L_1\boldsymbol{l}_{i1}\times\boldsymbol{F}_{Bi} - \boldsymbol{n}_{i1}. \tag{31}$$

## 4 Deformation Analyses of the links

The deformations of the components during the motion process will affect the accuracy of the machine. Compared with the links, the moving platform is more rigid, and its deformation can be negligible. Here, the deformations of the links will be investigated.

### 4.1 Deformation analysis of link $B_iC_i$

Both ends of link $B_iC_i$ are connected by passive frictionless revolute joints, where its bending deformation only occurs under the inertia moment of the link, which is relatively smaller than the constraints forces of the link. Besides, its maximum bending deformation occurs near the middle region of link $B_iC_i$, so its influence on the kinematic error of the end point of the link $B_iC_i$ is small. Therefore, only the tension and compression deformation of link $B_iC_i$, which can also be called axial deformation, is taken into consideration. The forces acting on link $B_iC_i$ is shown in Fig. 6, where $\boldsymbol{p}_{i2}(x)$ represents the distributed load on the link and can be described as

$$\boldsymbol{p}_{i2}(x) = \frac{-m_2\boldsymbol{a}_{i2x}}{L_2}, \tag{32}$$

where $\boldsymbol{a}_{i2x}$ is the acceleration of the point on link $B_iC_i$ at coordinate $x$.

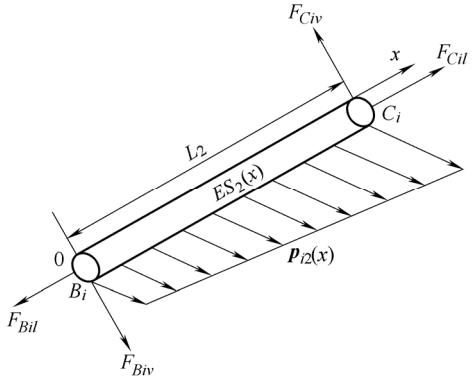


Fig. 6. Forces acting on link $B_iC_i$

The axial force of link $B_iC_i$ at coordinate $x$ can be written as

$$F_{d2x} = F_{Bil} - \int_0^x \left(\boldsymbol{l}_{i2}\bullet\boldsymbol{p}_{i2}(x)\right)\mathrm{d}x. \tag{33}$$

The axial deformation of link $B_iC_i$ can be described as

$$\delta L_{i2} = \int_0^{L_2}\frac{F_{d2x}dx}{ES_2} = \frac{L_2}{ES_2}\left(\frac{1}{2}m_2\boldsymbol{l}_{i2}\bullet\left(\boldsymbol{\varepsilon}_{i1}\times(L_1\boldsymbol{l}_{i1}) - \omega_{i1}^2L_1\boldsymbol{l}_{i1}\right) - \frac{1}{6}m_2\omega_{i2}^2L_2 + F_{Bil}\right), \tag{34}$$

where $S_2$ is the cross-sectional area of link $B_iC_i$, and $E$ is the elastic modulus.

### 4.2 Deformation analysis of link $A_iB_i$

Unlike link $B_iC_i$, one of the ends of link $A_iB_i$ is connected to the motor shaft, which can be considered as a fixed end. So it will also tend to be bending deformation except for axial deformation.

The forces acting on link $A_iB_i$ are shown in Fig. 7, where $\boldsymbol{p}_{i1}(x)$ represents the distributed load on the link and can be described as

$$\boldsymbol{p}_{i1}(x) = \frac{-m_1\boldsymbol{a}_{i1x}}{L_1}, \tag{35}$$

where $\boldsymbol{a}_{i1x}$ is the acceleration of the point on link $A_iB_i$ at coordinate $x$.

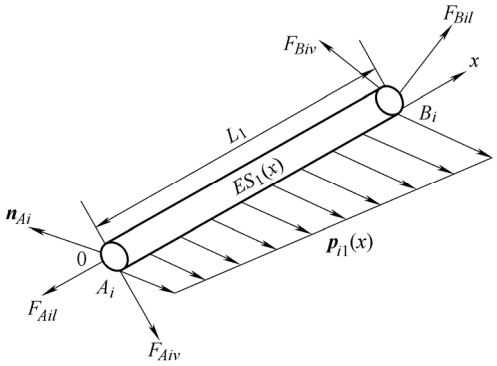


Fig. 7. Forces acting on link $A_iB_i$

The axial force of link $A_iB_i$ at coordinate $x$ can be written as

$$F_{d1x} = \int_x^{L_1}\left(\boldsymbol{l}_{i1}\bullet\boldsymbol{p}_{i1}(x)\right)\mathrm{d}x - \boldsymbol{l}_{i1}\bullet\boldsymbol{F}_{Bi}. \tag{36}$$

The axial deformation of link $A_iB_i$ can be described as

$$\delta L_{i1} = \int_0^{L_1}\frac{F_{d1x}dx}{ES_1} = \frac{L_1}{ES_1}\left(\frac{1}{3}m_1\omega_{i1}^2L_1 + \boldsymbol{l}_{i1}\bullet\boldsymbol{l}_{i2}^{\perp}F_{Biv} + \boldsymbol{l}_{i1}\bullet\boldsymbol{l}_{i2}F_{Bil}\right), \tag{37}$$

where $S_1$ is the cross-sectional area of link $A_iB_i$, and $\boldsymbol{l}_{i2}^{\perp} = \begin{pmatrix}-l_{i2y} & l_{i2x} & 0\end{pmatrix}^{\mathrm{T}}$.

The bending deformation diagram of link $A_iB_i$ is shown

in Fig. 8.

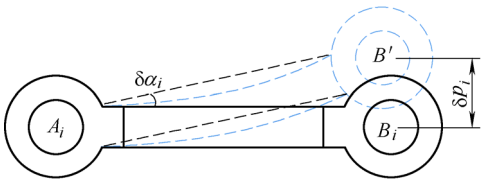


Fig. 8. Bending deformation diagram of link $A_iB_i$

The bending deformation of link $A_iB_i$ is caused by distributed load $\boldsymbol{p}_{i1}(x)$ and constraint force $\boldsymbol{F}_{Bi}$. In order to simplify the problem, the bending deformation can be solved by the superposition method.

Set point $A_i$ as a fixed end, the deflection of point $B_i$ under constraint force $\boldsymbol{F}_{Bi}$ can be described as

$$\delta p_i' = \frac{-\boldsymbol{l}_{i1}^{\perp} \cdot \boldsymbol{F}_{Bi} L_1^3}{3EI_1} = \frac{L_1^3}{3EI_1}\left(\boldsymbol{l}_{i1}^{\perp} \cdot \boldsymbol{l}_{i2}^{\perp} F_{Biv} + \boldsymbol{l}_{i1}^{\perp} \cdot \boldsymbol{l}_{i2} F_{Bil}\right), \quad (38)$$

where $I_1$ is the moment of inertia of link $A_iB_i$, and $\boldsymbol{l}_{i1}^{\perp} = \begin{pmatrix} -l_{i1y} & l_{i1x} & 0 \end{pmatrix}^{\mathrm{T}}$.

The deflection of point $B_i$ under distributed load $\boldsymbol{p}_{i1}(x)$ can be described as

$$\delta p_i'' = \int_0^{L_1} \frac{\boldsymbol{l}_{i1}^{\perp} \cdot \boldsymbol{p}_{i1}(x)}{6EI_1 L_1} x^2 (3L_1 - x)\mathrm{d}x = -\frac{11 m_1 \varepsilon_{i1} L_1^4}{120EI_1}. \quad (39)$$

Therefore, the total bending deformation of point $B_i$ is

$$\delta p_i = \frac{L_1^3}{3EI_1}\left(-\frac{11 m_1 \varepsilon_{i1} L_1}{40} + \boldsymbol{l}_{i1}^{\perp} \cdot \boldsymbol{l}_{i2}^{\perp} F_{Biv} + \boldsymbol{l}_{i1}^{\perp} \cdot \boldsymbol{l}_{i2} F_{Bil}\right). \quad (40)$$

The position error $\delta p_i$ of point $B_i$ caused by the bending deformation can be considered as the angular error $\delta\alpha_i$ of link $A_iB_i$, which can be described as

$$\delta\alpha_i = \delta p_i / L_1. \quad (41)$$

## 5 Accuracy Analysis of the Moving Platform

The deformations of links $A_iB_i$ and $B_iC_i$ will lead to kinematic errors of the moving platform, including the position errors( $\delta x$ and $\delta y$ ) and the rotation error( $\delta\gamma$ ). Taking the deformations of the links and these kinematic errors into account, Eq. (4) should be rewritten as

$$\boldsymbol{t} + \delta\boldsymbol{t} + \left({}^{O}\boldsymbol{R}_T + \delta\,{}^{O}\boldsymbol{R}_T\right){}^{T}\boldsymbol{C}_i = \boldsymbol{A}_i + (L_1 + \delta L_{i1})(\boldsymbol{l}_{i1} + \delta\boldsymbol{l}_{i1}) + (L_2 + \delta L_{i2})(\boldsymbol{l}_{i2} + \delta\boldsymbol{l}_{i2}), \quad (42)$$

where

$$\delta\boldsymbol{t} = \begin{pmatrix} \delta x & \delta y & 0 \end{pmatrix}^{\mathrm{T}},$$

$$\delta\,{}^{O}\boldsymbol{R}_T = (\boldsymbol{W}\boldsymbol{I})\delta\gamma,$$

$$\boldsymbol{W} = \begin{pmatrix} -\sin\gamma & -\cos\gamma & 0 \\ \cos\gamma & -\sin\gamma & 0 \\ 0 & 0 & 0 \end{pmatrix}, \quad \boldsymbol{I} = \begin{pmatrix} 1 & 0 & 0 \\ 0 & 1 & 0 \\ 0 & 0 & 1 \end{pmatrix},$$

$$\delta\boldsymbol{l}_{i1} = \delta\alpha_i \begin{pmatrix} -\sin\alpha_i & \cos\alpha_i & 0 \end{pmatrix}^{\mathrm{T}},$$

$$\delta\boldsymbol{l}_{i2} = \delta\beta_i \begin{pmatrix} -\sin\beta_i & \cos\beta_i & 0 \end{pmatrix}^{\mathrm{T}},$$

$\delta\beta_i$ is the angular error of link $B_iC_i$.

Subtraction of Eq. (4) from Eq. (42) and ignoring the higher order items yields

$$\delta\boldsymbol{t} + \delta\,{}^{O}\boldsymbol{R}_T\,{}^{T}\boldsymbol{C}_i = L_1\delta\boldsymbol{l}_{i1} + \boldsymbol{l}_{i1}\delta L_{i1} + L_2\delta\boldsymbol{l}_{i2} + \boldsymbol{l}_{i2}\delta L_{i2}. \quad (43)$$

Taking dot product of Eq. (43) with $\boldsymbol{l}_{i2}$ at both sides yields

$$\boldsymbol{l}_{i2} \cdot \left(\delta\boldsymbol{t} + \delta\,{}^{O}\boldsymbol{R}_T\,{}^{T}\boldsymbol{C}_i\right) = L_1\boldsymbol{l}_{i2}^{\mathrm{T}}\delta\boldsymbol{l}_{i1} + \boldsymbol{l}_{i2}^{\mathrm{T}}\boldsymbol{l}_{i1}\delta L_{i1} + \delta L_{i2}. \quad (44)$$

The relationships between the deformations of the links and the kinematic errors of the moving platform can be obtained from Eq. (44) as

$$\boldsymbol{E}_1\boldsymbol{D}_1 = \boldsymbol{E}_2\boldsymbol{D}_2, \quad (45)$$

where

$$\boldsymbol{D}_1 = \begin{pmatrix} \delta x & \delta y & \delta\gamma \end{pmatrix}^{\mathrm{T}},$$

$$\boldsymbol{D}_2 = \begin{pmatrix} \delta L_{11} & L_1\delta\alpha_1 & \delta L_{12} & \delta L_{21} & L_1\delta\alpha_2 & \delta L_{22} & \delta L_{31} & L_1\delta\alpha_3 & \delta L_{32} \end{pmatrix}^{\mathrm{T}},$$

$$\boldsymbol{E}_1 = \begin{pmatrix} l_{12x} & l_{12y} & u_1 \\ l_{22x} & l_{22y} & u_2 \\ l_{32x} & l_{32y} & u_3 \end{pmatrix} = \boldsymbol{P}^{\mathrm{T}},$$

$$\boldsymbol{E}_2 = \begin{pmatrix} w_1 & v_1 & 1 & 0 & 0 & 0 & 0 & 0 & 0 \\ 0 & 0 & 0 & w_2 & v_2 & 1 & 0 & 0 & 0 \\ 0 & 0 & 0 & 0 & 0 & 0 & w_3 & v_3 & 1 \end{pmatrix},$$

$$w_i = \boldsymbol{l}_{i1} \cdot \boldsymbol{l}_{i2}, v_i = \boldsymbol{l}_{i1}^{\perp} \cdot \boldsymbol{l}_{i2}.$$

From Eq. (45), the kinematic errors of the moving platform can be expressed as

$$\boldsymbol{D}_1 = \boldsymbol{E}_1^{-1}\boldsymbol{E}_2\boldsymbol{D}_2. \quad (46)$$

Eq. (46) can be deduced further on by replacing the deformations of the links with the expressions calculated above.

The relationship between $F_{Bil}$ and $F_{Cil}$ can be obtained from Eq. (19) as

$$F_{Bil} = F_{Cil} + \boldsymbol{l}_{i2} \bullet \boldsymbol{f}_{i2}. \tag{47}$$

Substituting $F_{Cil}$ for $F_{Bil}$ in Eqs. (34), (37) and (41) yields

$$\delta L_{i1} = \frac{L_1}{ES_1}\left(\boldsymbol{l}_{i1} \bullet \boldsymbol{l}_{i2} F_{Cil} + a_i\right), \tag{48}$$

$$\delta \alpha_i = \frac{L_1^2}{3EI_1}\left(\boldsymbol{l}_{i1}^{\perp} \bullet \boldsymbol{l}_{i2} F_{Cil} + b_i\right), \tag{49}$$

$$\delta L_{i2} = \frac{L_2}{ES_2}\left(F_{Cil} + c_i\right), \tag{50}$$

where

$$a_i = \frac{1}{3} m_1 \omega_{i1}^2 L_1 + \boldsymbol{l}_{i1} \bullet \boldsymbol{l}_{i2}^{\perp} F_{Biv} + \boldsymbol{l}_{i1} \bullet \boldsymbol{l}_{i2} \bullet \boldsymbol{l}_{i2} \bullet \boldsymbol{f}_{i2},$$

$$b_i = -\frac{11 m_1 \varepsilon_{i1} L_1}{40} + \boldsymbol{l}_{i1}^{\perp} \bullet \boldsymbol{l}_{i2}^{\perp} F_{Biv} + \boldsymbol{l}_{i1}^{\perp} \bullet \boldsymbol{l}_{i2} \bullet \boldsymbol{l}_{i2} \bullet \boldsymbol{f}_{i2},$$

$$c_i = \frac{1}{2} m_2 \boldsymbol{l}_{i2} \bullet \left[\boldsymbol{\varepsilon}_{i1} \times \left(L_1 \boldsymbol{l}_{i1}\right) - \omega_{i1}^2 L_1 \boldsymbol{l}_{i1}\right] - \frac{1}{6} m_2 \omega_{i2}^2 L_2 + \boldsymbol{l}_{i2} \bullet \boldsymbol{f}_{i2}.$$

Substituting Eqs. (48), (49) and (50) to Eq. (46) yields

$$\boldsymbol{D}_1 = \boldsymbol{E}_1^{-1} \boldsymbol{E}_2 \boldsymbol{K} \boldsymbol{E}_2^{\mathrm{T}} \boldsymbol{F} + \boldsymbol{N}, \tag{51}$$

where

$$\boldsymbol{F} = \begin{pmatrix} F_{C1l} & F_{C2l} & F_{C3l} \end{pmatrix}^{\mathrm{T}},$$

$$\boldsymbol{K} = \mathrm{diag}\left(\frac{L_1}{ES_1} \frac{L_1^3}{3EI_1} \frac{L_2}{ES_2} \frac{L_1}{ES_1} \frac{L_1^3}{3EI_1} \frac{L_2}{ES_2} \frac{L_1}{ES_1} \frac{L_1^3}{3EI_1} \frac{L_2}{ES_2}\right),$$

$$\boldsymbol{N} = \boldsymbol{E}_1^{-1} \boldsymbol{E}_2 \boldsymbol{K} \boldsymbol{G},$$

$$\boldsymbol{G} = \begin{pmatrix} a_1 & b_1 & c_1 & a_2 & b_2 & c_2 & a_3 & b_3 & c_3 \end{pmatrix}^{\mathrm{T}}.$$

Substituting Eq. (28) to (51) yields

$$\boldsymbol{D}_1 = \boldsymbol{E}_1^{-1} \boldsymbol{E}_2 \boldsymbol{K} \left(\boldsymbol{E}_1^{-1} \boldsymbol{E}_2\right)^{\mathrm{T}} \boldsymbol{Q} + \boldsymbol{N} = \boldsymbol{M} \boldsymbol{Q} + \boldsymbol{N}, \tag{52}$$

where $\boldsymbol{M} = \boldsymbol{E}_1^{-1} \boldsymbol{E}_2 \boldsymbol{K} \left(\boldsymbol{E}_1^{-1} \boldsymbol{E}_2\right)^{\mathrm{T}}$.

The foregoing analysis shows that the deformations of the links will lead to the position errors and the rotation error of the moving platform. Among those, the rotation error does not affect the accuracy of the center of the moving platform, so the accuracy of the machine can be measured by the total position error defined as

$$e = \sqrt{(\delta x)^2 + (\delta y)^2}. \tag{53}$$

## 6 Numerical Simulation

The geometrical and material parameters of the machine shown in Table 1 are used to study the accuracy of the machine when running the typical path.

**Table 1. Related parameters of the machine**

| Parameter | Value |
|---|---|
| Radius of the moving platform $r$ / mm | 150 |
| Radius of the fixed platform $R$ / mm | 600 |
| Length of link $A_iB_i$ $L_1$ / mm | 500 |
| Width of link $A_iB_i$ $b_1$ / mm | 30 |
| Height of link $A_iB_i$ $h_1$ / mm | 30 |
| Length of link $B_iC_i$ $L_2$ / mm | 500 |
| Width of link $B_iC_i$ $b_2$ / mm | 30 |
| Height of link $B_iC_i$ $h_2$ / mm | 30 |
| Thickness of the moving platform $H$ / mm | 30 |
| Density of the material $\rho$ / (g • mm$^{-3}$) | 7.9 |
| Elastic modulus of the material $E$ / GPa | 210 |

### 6.1 Workspace and motion planning

The workspace of the machine is presented in Fig. 9. In this workspace, a circle path is selected, with its center point at (0, 0) mm and a diameter of 350 mm.

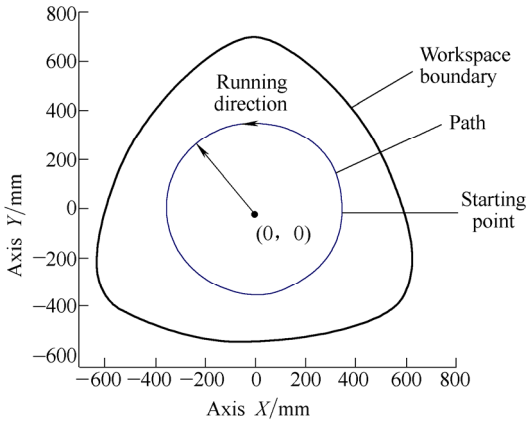


Fig. 9. Workspace and path

The acceleration characteristics of the moving platform when following this path should be planned. One of the most common methods is the S-Shape curve to impact, and the acceleration of the moving platform is given by

$$a = \begin{cases} \dfrac{2a_0}{t_\mathrm{d}} t & \left(0 < t \leqslant \dfrac{t_\mathrm{d}}{2}\right), \\ -\dfrac{2a_0}{t_\mathrm{d}} t + 2a_0 & \left(\dfrac{t_\mathrm{d}}{2} < t \leqslant t_\mathrm{d}\right), \\ 0 & \left(t_\mathrm{d} < t \leqslant T_\mathrm{t} - t_\mathrm{d}\right), \\ -\dfrac{2a_0}{t_\mathrm{d}} (t - T_\mathrm{t} + t_\mathrm{d}) & \left(T_\mathrm{t} - t_\mathrm{d} < t \leqslant T_\mathrm{t} - \dfrac{t_\mathrm{d}}{2}\right), \\ \dfrac{2a_0}{t_\mathrm{d}} (t - T_\mathrm{t}) & \left(T_\mathrm{t} - \dfrac{t_\mathrm{d}}{2} < t \leqslant T_\mathrm{t}\right), \end{cases} \tag{54}$$

where $a_0$ is the maximum acceleration, $t_d$ the time in acceleration and deceleration phases, and $T_t$ the total motion time. The velocity $v$ and displacement $s$ can be obtained by integration.

### 6.2 Simulation examples for the accuracy of the moving platform

Eq. (52) indicates that the precision of the moving platform will be affected by the performance of matrix $\boldsymbol{M}$. Matrix $\boldsymbol{M}$ is only defined by the geometrical parameters and the pose of the machine. Therefore, it can be used to optimize the design of the machine through further processing, such as normalization. The performance of matrix $\boldsymbol{M}$ can be evaluated by its condition number. A smaller condition number will ensure a better performance of the matrix. Here we can use its condition number for predicting the performance of this machine. The condition number of matrix $\boldsymbol{M}$ along the selected path is shown in Fig. 10.

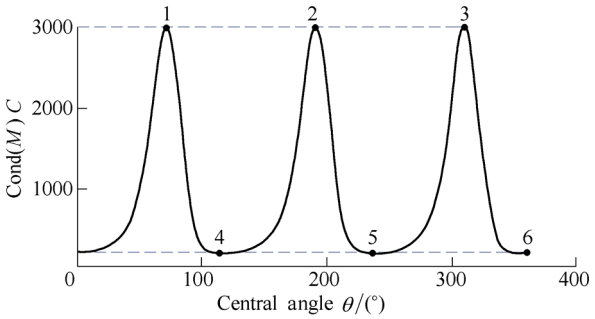


Fig. 10. Condition number of matrix $\boldsymbol{M}$ along the path

It can be seen that on points 1 to 3, where condition number reaches the maximum, matrix $\boldsymbol{M}$ has the worst performance, whereas matrix $\boldsymbol{M}$ has the best performance on points 4 to 6. The central angle of the circle path and the condition number of matrix $\boldsymbol{M}$ on each point are shown in Table 2.

**Table 2. Central angle and condition number on each point**

| Point number | Central angle $\theta$ / (°) | Cond($\boldsymbol{M}$) $C$ |
|---|---|---|
| 1 | 71.16 | 2993.04 |
| 2 | 191.16 | 2993.04 |
| 3 | 311.16 | 2993.04 |
| 4 | 116.04 | 166.75 |
| 5 | 236.04 | 166.75 |
| 6 | 356.04 | 166.75 |

To obtain a better comparison of the performance of the machine on the six points, the total position error graphs of the moving platform on each point under unit sphere force are given in Fig. 11. The size of the total position error graphs are expanded to 10 000 times to get a clear view.

Fig. 11 reflects the stiffness of the machine on each point at a certain extent. A longer length from the curve to the point means that the machine has a worse stiffness along the direction with longer length. It can be clearly seen that the size of the total position error graphs on points 1 to 3 are much larger than those on points 4 to 6. This indicates that it is easier for the machine to suffer from deformations on points 1 to 3 than on points 4 to 6 under the same force.

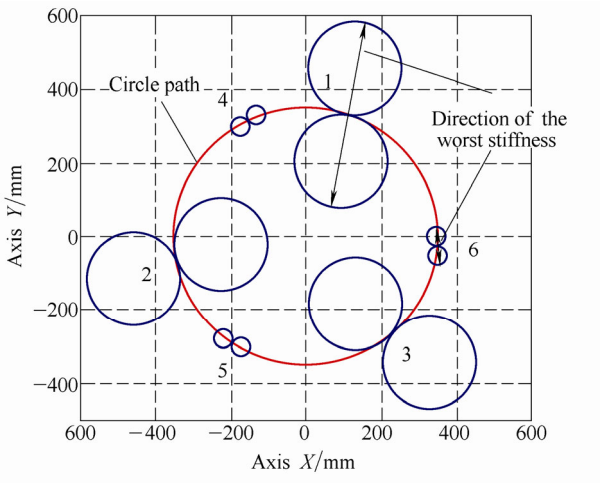


Fig. 11. Total position error graphs of the moving platform on each point

The total position errors of the moving platform when following the circle path with two different maximum accelerations are shown in Fig. 12. In this simulation, $t_d$ is 2s, and $a_0$ is 150 mm/s$^2$ and 200 mm/s$^2$, respectively. One can see that the maximum position error of the moving platform occurs near where the condition number of matrix $\boldsymbol{M}$ is also at its maximum. Moreover, the magnitude of the acceleration will have great influence on the accuracy of the machine. Though the maximum acceleration is increasing only from 150 mm/s$^2$ to 200 mm/s$^2$, the maximum position error of the moving platform nearly doubled.

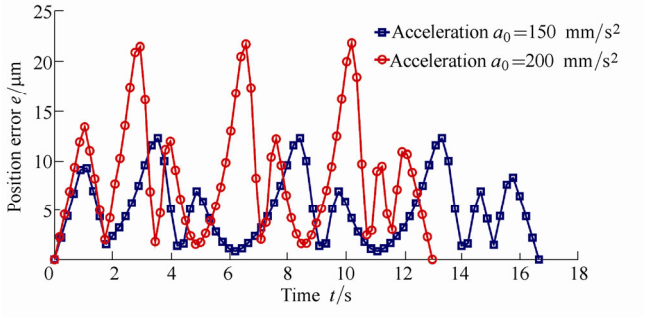


Fig. 12. Total position errors of the moving platform during motion process

### 6.3 Influence of external loads on the accuracy of the machine

The machine will inevitably suffer external loads during the motion process, so it is necessary to analyze its capacity in resisting their influence. The circle path is still selected for analyzing the influence of the external loads on the accuracy of the machine.

The direction with the worst stiffness of the machine along the path is shown in Fig. 13. The length of the line on each point represents the total position error of the moving platform under unit force along the direction with the worst stiffness, which can also be called flexibility. The sizes of the lines are expanded to 10 000 times to get a clear view. One can see that the direction of the worst stiffness varies along the path. It can be inferred that when the direction of the external loads coincides with the line, they will have a remarkable negative influence on the accuracy of the machine. So in order to decrease the negative influence of the external loads, they should be applied perpendicular to the direction of the worst stiffness as far as possible.

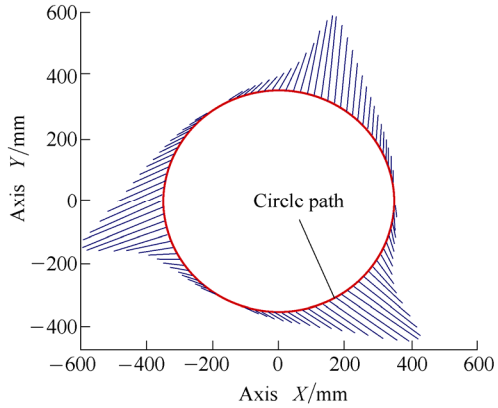


Fig. 13. Direction of the worst stiffness along the circle path

The flexibility of the machine along the circle path in directions $X$ and $Y$ is shown in Fig. 14 from which the stiffness performance of the machine on directions $X$ and $Y$ can be clearly obtained.

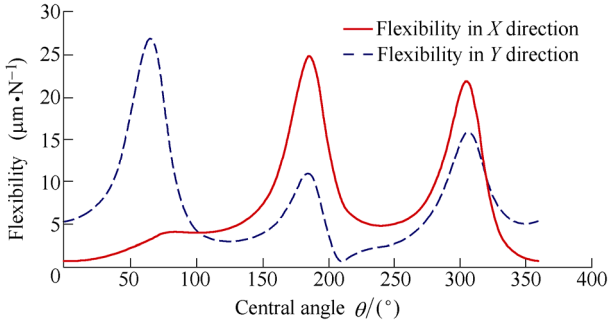


Fig. 14. Flexibility of the machine along the circle path in direction $X$ and $Y$

An external load of 1 N is applied separately on the center of the moving platform in direction $X$ and $Y$ during the motion process. In this simulation, the maximum acceleration $a_0$ is 200 mm/s$^2$. The total position errors of the moving platform without external load and under external load are all given in Fig. 15. The accuracy of the machine under external load is clearly decreased in the region where its flexibility is relatively large.

In the previous simulation, the inertia forces are also acting as external loads. In order to reduce their influence, the magnitude of the external load is increased to 10 N. The total position errors of the moving platform under such external load in direction $X$ and $Y$ are shown in Fig. 16. It can be clearly seen that the curves are almost in accordance with the curves of the flexibility of the machine in $X$ and $Y$ direction in Fig. 14.

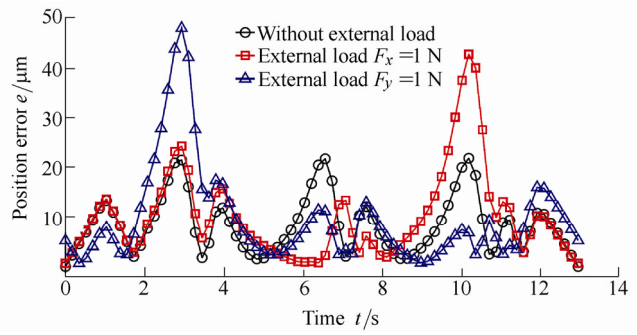


Fig. 15. Total position errors of the moving platform under force 1N in $X$ or $Y$ direction

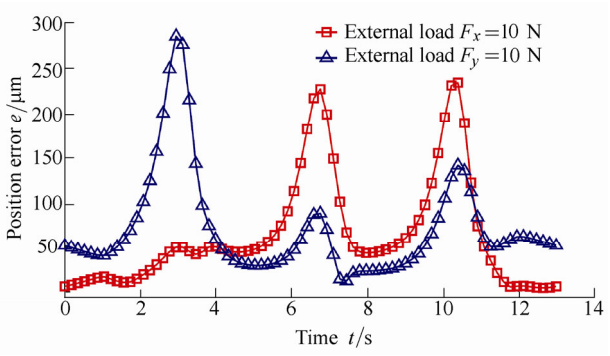


Fig. 16. Total position errors of the moving platform under force 10 N in $X$ or $Y$ direction

## 7 Conclusions

(1) Based on the dynamic model constructed by the Newton-Euler method, a simple explicit expression is derived to calculate the position error of the machine taking into consideration the deformations of the links.

(2) The running parameters, especially the magnitude of the maximum acceleration, will have great influence on the accuracy of the machine.

(3) The external loads will deteriorate the accuracy of the machine tremendously when their direction coincides with the direction of the worst stiffness of the machine.

(4) The method can be applied to the other PKMs and serial machines to analyze their running accuracy. It also provides a feasible solution for the design optimization as well as selection of running parameters of the machine.

## References

[1] WECH M, STAIMER D. Parallel kinematic machine tools—current state and future[J]. *CIRP Annals-Manufacturing Technology*, 2012, 51(2): 671–683.

[2] LI Yangmin, XU Qingsong. Kinematic analysis of a 3-PRS parallel manipulator[J]. *Robotics and Computer-Integrated Manufacturing*, 2007, 23(4): 395–408.

[3] LEBRET G, LIU K, LEWIS F L. Dynamic analysis and control of a Stewart platform manipulator[J]. *Journal of Robotic System*, 1993, 10(5): 629–655.
[4] TANG Xiaoqiang, WANG Jinsong, GAO Men. Kinematic calibration of gantry hybrid machine tool based on estimation error and local measurement information[J]. *International Journal of Advanced Manufacturing*, 2005, 26(4): 382–390.
[5] YAO Rui, ZHU Wenbai, HUANG Peng. Accuracy analysis of stewart platform based on interval analysis method[J]. *Chinese Journal of Mechanical Engineering*, 2013, 26(1): 29–34.
[6] BIAN Bian, HUANG Hai. Integrated design for configuration/ vibration control of hexapod platform[J]. *Chinese Journal of Mechanical Engineering*, 2009, 45(11): 72–77. (in Chinese)
[7] SONG J, MOU J I, KING C. Error modeling and compensation for parallel kinematic machines[C]//*The 1st European-American forum on Parallel Kinematic Machine*, Milan, Italy, 1999: 171–187.
[8] BRIOT S, BONEV I A. Are parallel robots more accurate than serial robots[J]. *Transactions of the Canadian Society for Mechanical Engineering*, 2007, 31(4): 445–455.
[9] BONEV I A, ZLATANOV D, GOSSELIN C M. Singularity analysis of a 3-DOF planar parallel mechanism via screw theory[J]. *Journal of Mechanical Design*, 2003, 125(3): 573–581.
[10] JOUBAIR A, SLAMANI M, BONEV I A. A novel XY-Theta precision table and a geometric procedure for its kinematic calibration[J]. *Robotics and Computer-Integrated Manufacturing*, 2012, 28(1): 57–65.
[11] JOUBAIR A, SLAMANI M, BONEV I A. Kinematic calibration of a five-bar planar parallel robot using all working modes[J]. *Robotics and Computer-Integrated Manufacturing*, 2013, 29(4): 15–25.
[12] CHANG Peng, LI Chengrong, LI Tiemin. Kinemaitc Calibration and forecast error compensation of a 2-DOF planar manipulator[J]. *Chinese Journal of Mechanical Engineering*, 2011, 24(6): 992–998.
[13] YU Yueqing, DU Zhaocai, YANG Jianxin, et al. An experimental study on the dynamics of a 3-RRR flexible parallel robot[J]. *IEEE Transactions on Robotics*, 2011, 27(5): 992–997.
[14] BRIOT S, BONEV I A. Accuracy analysis of 3-DOF planar parallel robots[J]. *Mechanism and Machine Theory*, 2008, 43(4): 445–458.
[15] DWIVEDY S K, EBERHARD P. Dynamic analysis of flexible manipulators, a literature review[J]. *Mechanical and Machine Theory*, 2006, 41(7): 749–777.
[16] PIRAS G, CLEGHORN W L, MILLS J K. Dynamic finite-element analysis of a planar high-speed, high-precision parallel manipulator with flexible links[J]. *Mechanism and Machine Theory*, 2005, 40(7): 849–862.
[17] ZHANG Xuping, MILLS J K, CLEGHORN W L. Dynamic modeling and experimental validation of a 3-PRR parallel manipulator with flexible intermediate links[J]. *Journal of Intelligent and Robotic Systems*, 2007, 50(4): 323–340.
[18] WANG Xiaoyun, MILLS J K. FEM dynamic model for active vibration control of flexible linkages and its application to a planar parallel manipulator[J]. *Applied Acoustics*, 2005, 66(10): 1151–1161.
[19] ZHOU Z, XI J, MECHEFSKE C K. Modeling of a fully flexible 3PRS manipulator for vibration analysis[J]. *Journal of Mechanical Design*, 2006, 128(2): 403–412.
[20] GOSSELIN C M. The optimum design of robotic manipulators using dexterity indices[J]. *Robotics and Autonomous Systems*, 1992, 9(4): 213–226.
[21] GOSSELIN C M, ANGELES J. A global performance index for the kinematic optimization of robotic manipulators[J]. *Journal of Mechanical Design*, 1991, 113(3): 220–226.
[22] YU A, BONEV I A, ZSOMBOR-MURRAY P. Geometric approach to the accuracy analysis of a class of 3-DOF planar parallel robots[J]. *Mechanism and Machine Theory*, 2008, 43(3): 364–375.
[23] MERLET J P. Computing the worst case accuracy of a PKM over a workspace or a trajectory[C]//*The 5th Chemnitz Parallel Kinematics Seminar*, Chemnitz, Germany, 2006: 83–96.
[24] BRIOT S, BONEV I A. A pair of measures of rotational error for axisymmetric robot end-effectors[C]//*Advances in Robot Kinematics*, *11th International Symposium*, France, 2008: 345–352.
[25] MERLET J P. Jacobian, manipulability, condition number, and accuracy of parallel robots[J]. *Journal of Mechanical Design*, 2006, 128(1): 199–206.
[26] ARSENAULT M, BOUDREAU R. Synthesis of planar parallel mechanisms while considering workspace, dexterity, stiffness and singularity avoidance[J]. *Journal of Mechanical Design*, 2006, 128(1): 69–78.
[27] ARAKELIAN V H, SMITH M R. Design of planar 3-DOF 3-RRR reactionless parallel manipulators[J]. *Mechantronics*, 2008, 18(10): 601–606.
[28] SHAO Zhufeng, TANG Xiaoqiang, CHEN Xu, et al. Inertia match of a 3-RRR reconfigurable planar parallel manipulator[J]. *Chinese Journal of Mechanical Engineering*, 2009, 22(6): 791–799.

## Biographical notes

WANG Liping, born in 1967, is currently a professor and a PhD candidate supervisor at *Manufacturing Engineering Institute*, *Department of Mechanical Engineering*, *Tsinghua University, China*. He received his PhD degree from *Jilin University of Technology*, *China*, in 1997. His research interests include advanced equipment and parallel kinematic machines.
E-mail: lpwang@tsinghua.edu.cn

JIANG Yao, born in 1989, is currently a PhD candidate at *Manufacturing Engineering Institute*, *Department of Mechanical Engineering*, *Tsinghua University*, *China*. He received his bachelor degree from *Nanjing University of Technology*, *China*, in 2011. His research interests include dynamics and control of redundant kinematic parallel machines.
E-mail: jiangyao11@mails.tsinghua.edu.cn

LI Tiemin, born in 1971, is currently an associate research fellow at *Manufacturing Engineering Institute*, *Department of Mechanical Engineering*, *Tsinghua University*, *China*. He received his PhD degree from *Tsinghua University*, *China*, in 2000. His interests include robotics and parallel kinematic machines.
E-mail: litm@tsinghua.edu.cn